

Evolving AMOC multidecadal variability under different CO₂ forcings

Xiaofan Ma^{1,7} · Wei Liu² · Natalie J. Burls³ · Changlin Chen⁴ · Jun Cheng⁵ · Gang Huang^{1,6,7} · Xichen Li⁸

Received: 3 October 2020 / Accepted: 9 March 2021 / Published online: 18 March 2021 © The Author(s), under exclusive licence to Springer-Verlag GmbH Germany, part of Springer Nature 2021

Abstract

Multidecadal variability of the Atlantic Meridional Overturning Circulation (AMOC) plays a vital role in Earth's climate variability. Climate change has the potential to alter the causes and characteristics of AMOC multidecadal variability. Here we use a coupled climate model to simulate AMOC multidecadal variability under three distinct atmospheric CO_2 concentrations: Last Glacial Maximum, preindustrial, and 4 × preindustrial levels. Firstly, we discover that AMOC multidecadal variability exhibits a shortened period and a reduced amplitude with increasing atmospheric CO_2 . We find that these changes in AMOC variability are largely related to enhanced ocean stratification in the subpolar North Atlantic with increasing CO_2 which in turn changes the characteristics of westward propagating oceanic baroclinic Rossby waves. Our analysis indicates that the shortened period is primarily due to the increased speed of free oceanic Rossby waves, and the reduced amplitude is mainly due to the reduced magnitude of atmospherically-forced oceanic Rossby waves. Mean flow effects, in the form of eastward mean zonal advection and westward geostrophic self-advection, need to be considered as they largely increase the speed of Rossby waves and hence allow for a better estimate of the changes in the period and amplitude of AMOC variability. Secondly, to explore the possible linkage between atmospheric variability and AMOC fluctuations under each CO_2 concentration in a qualitative manner, we analyze the relationship between the North Atlantic Oscillation (NAO) and the AMOC and find a significant negative correlation between the two only under the preindustrial levels where the NAO leads the AMOC by 3–11 years.

Keywords Atlantic Meridional Overturning Circulation \cdot Multidecadal variability \cdot CO₂ change \cdot Oceanic baroclinic Rossby waves \cdot Mean flow effects \cdot North Atlantic Oscillation

1 1 Introduction

The Atlantic Meridional Overturning Circulation (AMOC) is an important component of the global ocean circulation consisting of a warm, northward near-surface flow and a cold, southward return flow at depth. Through strong

northward heat and freshwater transports, the AMOC and its variability influence the climate over the North Atlantic and surrounding regions (Liu et al. 2017, 2020; Ma et al. 2020), such as Atlantic hurricanes (Knight et al. 2006; Zhang and Delworth 2006), North American and European summer climate (Enfield et al. 2001; Sutton and Hodson 2005), and

- ☐ Gang Huang hg@mail.iap.ac.cn
- State Key Laboratory of Numerical Modeling for Atmospheric Sciences and Geophysical Fluid Dynamics, Institute of Atmospheric Physics, Chinese Academy of Sciences, 100029 Beijing, China
- Department of Earth Sciences and Planetary Sciences, University of California Riverside, Riverside, CA 92521, USA
- Department of Atmospheric, Oceanic, and Earth Sciences, George Mason University, Fairfax, VA 22030, USA
- Department of Atmospheric and Oceanic Sciences, Institute of Atmospheric Sciences, Fudan University, Shanghai, China

- Polar Climate System and Global Change Laboratory, Nanjing University of Information Science and Technology, Nanjing 210044, China
- Laboratory for Regional Oceanography and Numerical Modeling, Qingdao National Laboratory for Marine Science and Technology, Qingdao 266237, China
- University of Chinese Academy of Sciences, Beijing 100049, China
- International Center for Climate and Environment Sciences, Institute of Atmospheric Physics, Chinese Academy of Sciences, Beijing 10029, China



India/Sahel rainfall (Knight et al. 2006; Zhang and Delworth 2006). During past climates, the AMOC has been suggested to play an important role in abrupt climate changes such as those during the last deglaciation (McManus et al. 2004; Liu et al. 2009). For future climate, owing to its intense variability on decadal to centennial timescales, the AMOC potentially serves as a key factor in decadal climate prediction (Griffies and Bryan 1997; Msadek et al. 2010; Latif and Keenlyside 2011; Zhang and Zhang 2015; Zhang et al. 2019).

Given the relatively short period of direct AMOC observations (e.g., the 1-2 decades of observations from the RAPID array at 26.5° N; Srokosz and Bryden 2015), previous studies on AMOC variability primarily rely on model simulations. The nature of AMOC variability has proven to be model dependent with numerous studies giving rise to a diversity of mechanisms driving AMOC variability on decadal to centennial timescales (see reviews, Liu 2012; Buckley and Marshall 2016). Many of these studies have indicated that AMOC variability acts mainly as an internal ocean mode. For example, studies with ocean-only models under prescribed surface forcing have illustrated clear, selfexcited, interdecadal AMOC variability generated by baroclinic instability (Colin de Verdiere and Huck 1999; Huck and Vallis 2001; Huck et al. 2001; Te Raa and Dijkstra 2002; Arzel et al. 2018; Arzel and Huck 2020) or thermohaline instability (Weaver et al. 1991; Yin and Sarachik 1995). On the other hand, in fully-coupled models, multidecadal AMOC variability was found to be driven by density anomalies in deep convection regions (Delworth et al. 1993; Dai et al. 2005). Furthermore, there has been growing recognition that atmospheric forcing can excite significant AMOC multidecadal variability and play an important role in maintaining the amplitude of oscillations (Delworth et al. 1993; Griffies and Tziperman 1995; Delworth and Greatbatch 2000; Dong and Sutton 2005; Danabasoglu 2008; Kwon and Frankignoul 2012; Danabasoglu et al. 2012).

Previous studies have identified mechanisms driving AMOC variability at different frequencies. They are either internal ocean modes or ocean processes affected by the atmosphere. A series of studies have suggested that AMOC multidecadal variability with periods longer than 40 years is controlled by freshwater exchange between the North Atlantic and the Arctic Ocean/Nordic Sea (Delworth et al. 1997; Jungclaus et al. 2005; Hawkins and Sutton 2007; Frankcombe et al. 2010; Frankcombe and Dijkstra 2011; Ortega et al. 2017; Liu et al. 2019). Many other studies have focused on AMOC variability with a 20-30 year period and linked it to the westward propagation of large-scale temperature or density anomalies in the North Atlantic as seen in observed ocean temperature (Frankcombe et al. 2008), observed sea surface height (Frankcombe and Dijkstra 2009), idealized ocean models (Te Raa and Dijkstra 2002; Dijkstra et al.

2006), and general circulation models (Frankcombe and Dijkstra 2009, 2011; Frankcombe et al. 2010; Buckley et al. 2012; Tulloch and Marshall 2012; Sévellec and Fedorov 2013, 2015; Ortega et al. 2015; Arzel et al. 2018; Arzel and Huck 2020). These westward propagating temperature signals were attributed to baroclinic Rossby waves or the socalled thermal Rossby wave in the ocean (Frankcombe et al. 2008; Buckley et al. 2012). Recent studies further showed that the westward propagation of these temperature or density signals is produced by interactions between mean zonal advection, geostrophic self-advection, and ocean baroclinic Rossby waves (Sévellec and Fedorov 2013, 2015; Ortega et al. 2015; Muir and Fedorov 2017). Additionally, several studies have linked the strong ~ 20-year AMOC variability to an ocean-sea ice-atmosphere coupled mode as seen in the IPSL-CM5A-LR model (Escudier et al. 2013; Ortega et al. 2015). The basin-wide baroclinic Rossby waves propagating in the ocean subsurface and the ocean-sea ice-atmosphere coupled mode at the ocean surface have been discovered to couple together via deep convection and the East Greenland Current, which may explain the simulated strong ~ 20-year AMOC periodicity (Ortega et al. 2015).

Several studies have highlighted the central role of ocean-atmosphere coupling for AMOC variability. On centennial timescale, an interaction between the AMOC and the Inter Tropical Convergence Zone has been found in the HadCM3, KCM, and MPI-ESM models (Vellinga and Wu 2004; Menary et al. 2012) while a modest positive feedback between Southern Ocean westerly winds and AMOC variations was identified in GFDL-CM2.1 model (Delworth and Zeng 2008). On the multidecadal timescales, feedbacks between the NAO and AMOC have been investigated in the ECHAM1/LSG model (Timmermann et al. 1998) while another similar feedback was found between the East Atlantic Pattern and AMOC in the IPSL-CM4 model (Msadek and Frankignoul 2009). Combined effects of NAO and East Atlantic Pattern on driving AMOC are found in CNRM-CM5 model (Ruprich-Robert and Cassou 2015). In fact, previous studies have not reached an agreement on whether AMOC multidecadal variability is an ocean response to atmospheric forcing or an ocean-atmosphere coupled mode (see review Zhang et al. 2019).

The broad diversity of timescales and mechanisms among models presents a great challenge to better understand the internal variability of the climate system. There are perhaps more challenges when we consider that potential alterations in internal variability may happen if large changes in external forcing occur, especially under the current strong global warming. To date there has been little focus on the changes in both the period and amplitude of AMOC variability under different background climates. Several studies have found a decrease in AMOC variability in a warming world due to increasing CO₂ (Drijfhout et al. 2008; MacMartin



et al. 2016; Cheng et al. 2016; Armstrong et al. 2017). In particular, the decreased AMOC variability is associated with enhanced ocean stratification (MacMartin et al. 2016; Cheng et al. 2016; Armstrong et al. 2017) and the resulting acceleration of ocean baroclinic Rossby waves (Cheng et al. 2016). Nevertheless, these studies were primarily based on either simulations under multiple climate forcings (Drijfhout et al. 2008; Cheng et al. 2016), or simulations solely under a $\rm CO_2$ increase relative to preindustrial level (MacMartin et al. 2016; Armstrong et al. 2017). It remains unclear how and why AMOC multidecadal variability alters under different atmospheric $\rm CO_2$ forcings, especially considering the low to high $\rm CO_2$ climates that the Earth has experienced in the past or might expect in the future.

To address this gap, this study focuses on two key scientific questions: (1) How does AMOC multidecadal variability change under three atmospheric CO₂ concentrations ranging from the Last Glacial Maximum (LGM) level, to the preindustrial level, to the $4 \times$ preindustrial level; and (2) what are the physical mechanisms responsible for the change. Here we use a coupled model to address these two issues through sensitivity experiments forced by the three atmospheric CO₂ concentrations. The paper is organized as follows. The model and experiments are described in Sect. 2. Section 3 presents the results on how AMOC multidecadal variability evolves across our simulations, the mechanisms driving the evolution in AMOC variability, and the oceanic temperature phase change related to AMOC oscillations. The effect of atmospheric variability on the AMOC under each CO₂ concentrations is also investigated in this section. Conclusion and discussion are given in Sect. 4.

2 Model and experiments

The coupled climate model used in this study is the Community Earth System Model (CESM) version 1.0.4 with Carbon Nitrogen (CN), which is denoted as CESM1-CN in the rest of the paper. The atmosphere component is the Community Atmosphere Model version 4 (CAM4) (Neale et al. 2010) with a T31 spectral dynamical core, which has a nominal 3.75° horizontal resolution and 26 vertical layers. The land component is the Community Land Model version 4 (CLM4) (Lawrence et al. 2012) and is on the same horizontal grid as the atmosphere component. The ocean component is the Parallel Ocean Program version 2 (POP2) (Smith et al. 2010) with a gx3v7 resolution, which adopts a nominal 3° irregular horizontal resolution and 60 vertical layers (Shields et al. 2012). The horizontal grid is finer near Greenland and in the Arctic (~1°), which enables POP2 to well resolve high-latitude ocean topography. The sea ice component is the Community Ice Code version 4 (CICE4)

(Holland et al. 2012) and shares the same horizontal resolution with the ocean component.

In CESM1-CN, the AMOC (ψ) is represented by integrating the meridional velocity (ν) zonally and vertically in the Atlantic:

$$\bar{\Psi}(y,z) = \int_{X_{w}}^{X_{E}} \int_{-z}^{0} v(x,y,z) dz dx$$
 (1)

where x, y, and z are the zonal, meridional, and vertical coordinates. X_W and X_E denote the longitudes of the western and eastern boundaries of the Atlantic, respectively. At each latitude, we choose the maximum streamfunction below 500 m as the AMOC index. In the preindustrial control run, the AMOC index at 26.5° N is around 15 Sv (1 Sv = 10^6 m³ s⁻¹), which is consistent with the RAPID array observation at this latitude (Srokosz and Bryden 2015).

Based on the CESM1-CN preindustrial control run (piCO₂, 280 ppm), we conduct two parallel sensitivity experiments by abruptly altering the atmospheric CO₂ concentrations to the LGM level (LGMCO₂, 185 ppm) and 4 × the preindustrial level (4 \times CO₂, 1120 ppm), respectively. All other forcings remain the same as in the preindustrial control run. In response to the CO₂ decrease and increase, the AMOC quickly strengthens (weakens) during the first 100 years of the LGMCO₂ ($4 \times CO_2$) experiment and slowly evolves afterward (Fig. 1d). In both experiments, the AMOC strength reduces after the initial 100-year adjustment and becomes relatively steady after ~300 years (Fig. 1d). Note that in the $4 \times CO_2$ simulation, the wind-driven upper ocean is in a state of near equilibrium but the deep ocean is still slowly adjusting on 1000 year plus timescales. The evolution of the AMOC in the LGMCO₂ and $4 \times CO_2$ experiments is similar to the studies using other versions of the same model and exploring AMOC changes after an abrupt atmospheric CO₂ change (Brady et al. 2013; Zhu et al. 2015). In these studies, the AMOC shows relatively fast adjustments in the first 2–3 centuries after the CO₂ change and comes into steady status in the later centuries. Compared to the piCO₂ (Fig. 1b), the mean AMOC in LGMCO₂ has a similar magnitude but extends to deeper layers (Fig. 1a), while the mean AMOC in $4 \times CO_2$ shows a very weak and shallow pattern and is confined to the top ~ 1500 m layers and south of 40° N (Fig. 1c).

To examine the response of AMOC multidecadal variability to abrupt CO_2 changes after the initially fast ocean adjustment, we choose 500 years (301–800 years after CO_2 changes) in LGMCO₂ and 4 × CO_2 experiments together with a 500-year simulation from pi CO_2 for the following analyses. All the data are detrended over the selected 500 years by a linear least-square fit before analyses to remove



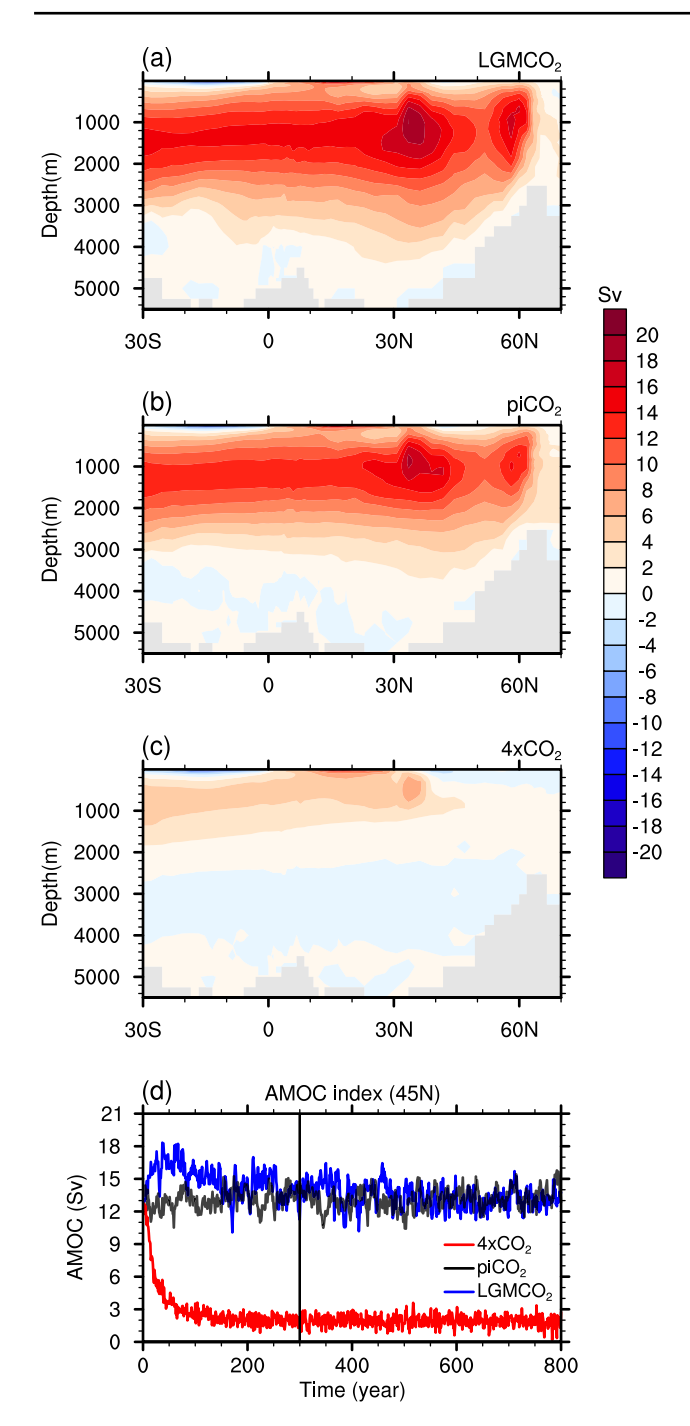


Fig. 1 The mean meridional overturning streamfunction in the Atlantic in the **a** LGMCO₂, **b** piCO₂, and **c** $4 \times \text{CO}_2$ simulations. **d** Time series of AMOC index at 45° N in the LGMCO₂ (blue), piCO₂ (black), and $4 \times \text{CO}_2$ (red) simulations. The vertical black line denotes the start year of the 500-year time span (301–800) analyzed in the present study

any climate drift in model simulations. Annual-mean data for multiple variables are utilized except that March climatological data is used for ocean mixed layer depth (Hu

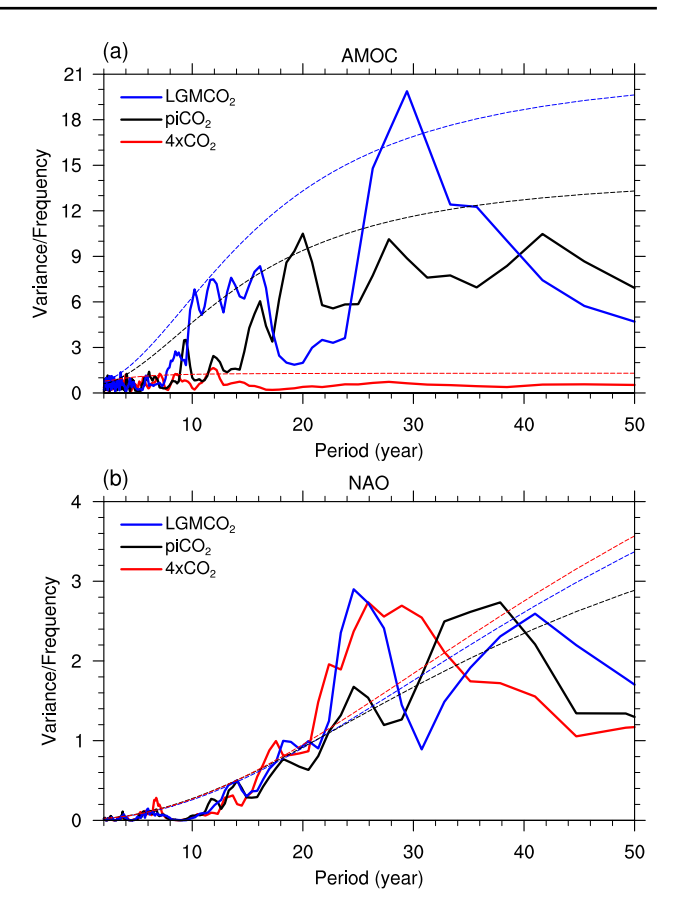


Fig. 2 Power spectrum for the 500-year **a** AMOC index at 45° N and **b** NAO index in the LGMCO₂ (blue), piCO₂ (black), and $4 \times \text{CO}_2$ (red) simulations. The NAO index here is adopted as the principal component time series of the leading empirical orthogonal function of annual mean sea level pressure anomalies over the Atlantic sector (10° N–80° N, 100° W–40° E). Dash lines denote the 95 % confidence level. A 9-year running mean is applied to NAO index before calculating the power spectrum

et al. 2008; Liu and Liu 2013). The student's t-test is used for the statistical significance test on the cross-correlation, with the effective degree of freedom calculated as in Zhang and Wang (2013).

3 Results

3.1 The evolving AMOC variability

We first explore AMOC multidecadal variability in the CESM1-CN preindustrial control run and the two sensitivity experiments. We examine the power spectrum of the 500-year AMOC index at 45° N where the AMOC variability is customarily large, and convenient for the comparison among models (Muir and Fedorov 2017; Menary and Wood 2018). We find significant peaks in AMOC variability at periods around 29.4, 20.0, and 11.9 years within the LGMCO₂,



piCO₂, and $4 \times \text{CO}_2$ simulations respectively, with the magnitude of these peaks declining in this order (Fig. 2a). That is to say, AMOC multidecadal variability weakens and its major period diminishes as CO₂ increases from the LGM level to the $4 \times$ preindustrial level. These characteristics are consistent with the results from previous studies (Drijfhout et al. 2008; MacMartin et al. 2016; Cheng et al. 2016; Armstrong et al. 2017).

These changes in AMOC variability are closely linked to the changes in ocean stratification which serves as a measure of ocean vertical stability and can be represented by the buoyancy (Brunt-Väisälä) frequency (N²). Stronger stratification is indicative of a greater vertical density gradient (larger N²) and hence weaker convective activity (Sgubin et al. 2017). Along with the decline in period and magnitude of AMOC multidecadal variability, we also find an increase in ocean stratification in the subpolar North Atlantic under increasing CO₂. Figure 3 displays the vertical profiles of buoyancy frequency and potential density in the three simulations averaged over the subpolar North Atlantic $(45^{\circ} \text{ N--}60^{\circ} \text{ N}, 80^{\circ} \text{ W--}0^{\circ})$, where the vertically-integrated buoyancy frequency has large anomalies (not shown) tightly related to the locally strong AMOC variations. All three vertical profiles show strongly stratified thermocline waters lie between weaker stratified mixed layers and deep waters (Fig. 3a). Increasing CO₂ alters these profiles by enhancing the buoyancy frequency and decreasing the density throughout the water column, making the water column more stratified as seen from the enlarged density difference between surface and subsurface waters, especially in the top 1000 m (Fig. 3b). The change in vertical stratification from piCO₂ to $4 \times CO_2$ is much larger than that from LGMCO₂ to piCO₂, which is likely due to the larger CO₂ increase in the former transition than the latter.

We further examine the propagation features of temperature anomalies that are related to the modes of AMOC multidecadal variability. For each simulation, we average the temperature anomalies over 45° N-60° N and 0-1000 m depth in the Atlantic basin with a band-pass filter applied around the spectral peak of AMOC variability (the peak at 29.4, 20.0, and 11.9 years respective for LGMCO₂, piCO₂, and $4 \times$ CO_2). We find robust westward propagation of temperature anomalies across the central-western parts of the Atlantic basin in all three simulations (Fig. 4). From LGMCO₂ to piCO₂, and to $4 \times CO_2$, the westward propagating temperature signals exhibit decreased magnitude but increased speed (Fig. 4), which is consistent with the changes in AMOC multidecadal variability. Note that the propagation of temperature signals varies with longitude and time. Eastward temperature propagations occur to the east of 20° W where the eastward mean flow possibly overwhelms the westward propagation of anomalies (e.g., Muir and Alexey 2017). To summarize, in our CESM1-CN simulations we observe altered AMOC multidecadal variability under increasing CO₂ and associated changes in ocean stratification and the westward propagation of temperature anomalies in the subpolar North Atlantic. Next, we will integrate all these findings using baroclinic Rossby wave theory to explain the possible mechanisms driving the changes in AMOC multidecadal variability across these simulations.

3.2 Mechanisms behind the changes in AMOC multidecadal variability

3.2.1 Period

Baroclinic Rossby wave theory links AMOC variability to the westward propagation of temperature or density anomalies in the North Atlantic (Buckley et al. 2012; Sévellec

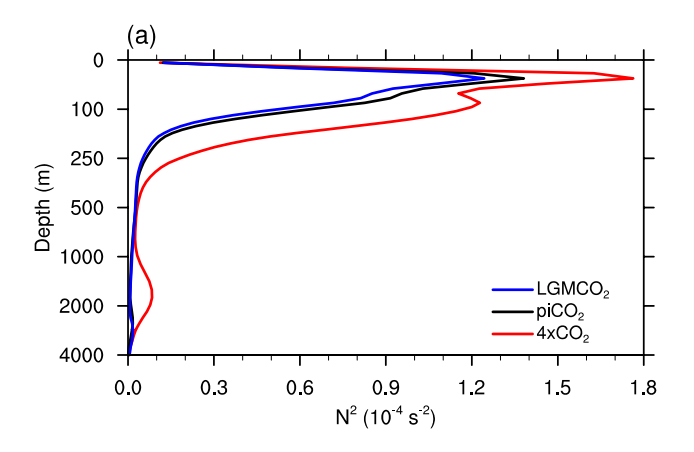
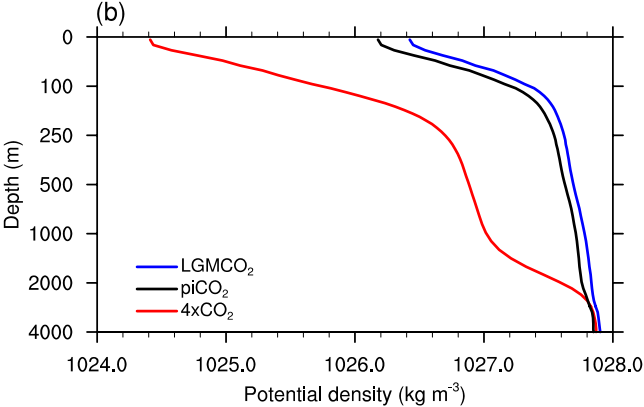


Fig. 3 Vertical profiles of **a** buoyancy frequency (N^2) and **b** potential density in the LGMCO₂ (blue), piCO₂ (black), and $4 \times CO_2$ (red) simulations, averaged over the subpolar North Atlantic (45° N–60° N,



 80° W–0°) and the 500-year period. Notice the unequal vertical scale is used to amplify the changes in the top 1000 m



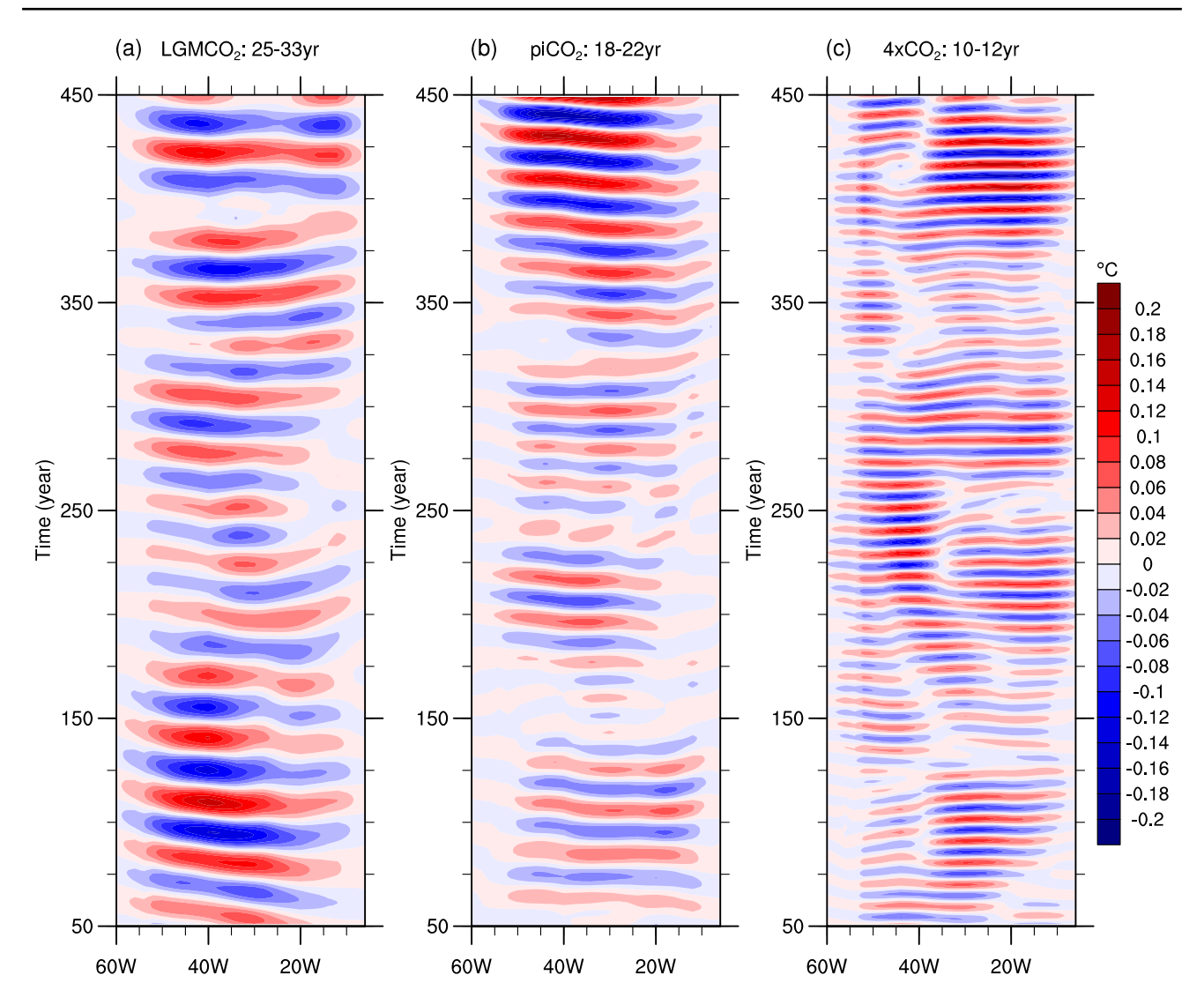


Fig. 4 Hovmöler diagrams showing the westward propagation of temperature anomalies during the 500 years analyzed in the **a** LGMCO₂, **b** piCO₂, and **c** $4 \times \text{CO}_2$ simulations. Temperatures are averaged over 45° N– 60° N, 0–1000 m. Time goes upward. A band-pass filter is

applied around AMOC spectral peaks in each simulation. The numbers on the top of each plot denote the spectral bands used for the band-pass filtering. There is 50-year loss on each end of the Y-axis in each plot due to the filtering

and Fedorov 2013, 2015; Ortega et al. 2015), which can be understood as the visible signals of westward propagating baroclinic Rossby waves. Stronger ocean stratification in a warming climate will induce faster westward-propagating baroclinic Rossby waves across the Atlantic basin, which could lead to alterations in both period and amplitude of AMOC multidecadal variability.

Following baroclinic Rossby wave theory, we examine the mechanisms behind the change in AMOC multidecadal variability in our simulations. We calculate the baroclinic Rossby wave speed in the three simulations based on an eigenvalue problem deduced from the linearized quasigeostrophic potential vorticity (QGPV) equation (Gill

1982), using the 500-year mean buoyancy frequency profiles averaged over 45° N– 60° N, 80° W– 0° . We first examine the simplest case for the free baroclinic Rossby wave in the ocean, without considering background zonal mean flow (U=0) and other forcings. The linearized QGPV equation can be written as

$$\partial_t \left[\partial_{xx} + \partial_{yy} + \partial_z \left(\frac{f_0^2}{N^2} \partial_z \right) \right] \psi + \beta \partial_x \psi = 0$$
 (2)

 ψ is the geostrophic streamfunction. β is the gradient of planetary vorticity (β -effect) and f_0 is the Coriolis



parameter. $N^2 = -\frac{g}{\rho_0} \frac{d\rho}{dz}$ denotes buoyancy frequency where ρ_0 is reference ocean density and ρ is the ocean density.

Setting $\psi = \varphi(z)\Psi(x, y)e^{-i\omega t}$, we obtain the equation for the vertical structure as

$$\frac{d}{dz} \left[\frac{f_0^2}{N(z)^2} \frac{d\varphi}{dz} \right] - \lambda \varphi = 0 \tag{3}$$

The eigenvalue $\lambda = \frac{\beta k}{\omega}$, where k is zonal wavenumber and ω is circular frequency. For specific f_0 and N^2 , we can get numerical solutions for eigenvalue λ and eigenfunction ϕ (Chelton et al. 1998). Accordingly, the phase speed value of the first baroclinic Rossby wave under the longwave assumption is

$$c = \frac{\omega}{k} = \frac{\beta}{\lambda} \tag{4}$$

The timescale for the first baroclinic Rossby wave to propagate across the basin is

$$T = \frac{L}{c} \tag{5}$$

where L is the mean width of the North Atlantic basin between 45° N–60° N ($L \approx 3700$ km). This timescale is thought to be critical in setting the major period of AMOC multidecadal variability (Kawase 1987; Johnson and Marshall 2002). Here we compute the propagating timescale based on the mode with two anomalies in opposite signs propagating westward together.

Figure 5 shows the impact of ocean stratification on the speed of the first baroclinic Rossby waves and the time scale for these waves to propagate across the Atlantic basin in the three simulations. With increasing atmospheric CO₂, ocean baroclinic Rossby waves accelerate due to the enhanced ocean stratification in the subpolar North Atlantic (Fig. 5a, blue). The acceleration of Rossby waves is more striking in the transition from piCO₂ to $4 \times CO_2$ relative to the transition from LGMCO₂ to piCO₂. As a consequence of the acceleration of Rossby waves, the time scale for waves traveling across the Atlantic basin decreases (Fig. 5b, blue), which is in general consistent with the shortened period of AMOC variability under increasing CO₂ conditions (Fig. 2a). Our calculation shows that the durations for Rossby waves traveling across the Atlantic basin in the LGMCO₂, piCO₂, and 4×CO₂ simulations are 59.8, 55.9, and 12.2 years, respectively (Fig. 5b, blue). These durations, however, do not accurately predict the AMOC variability periods of 29.4, 20.0, and 11.9 years as estimated from the power spectrum peaks of AMOC index at 45°N, especially in the cases of LGMCO₂ and piCO₂ (Fig. 5b, black). Thus, it is reasonable

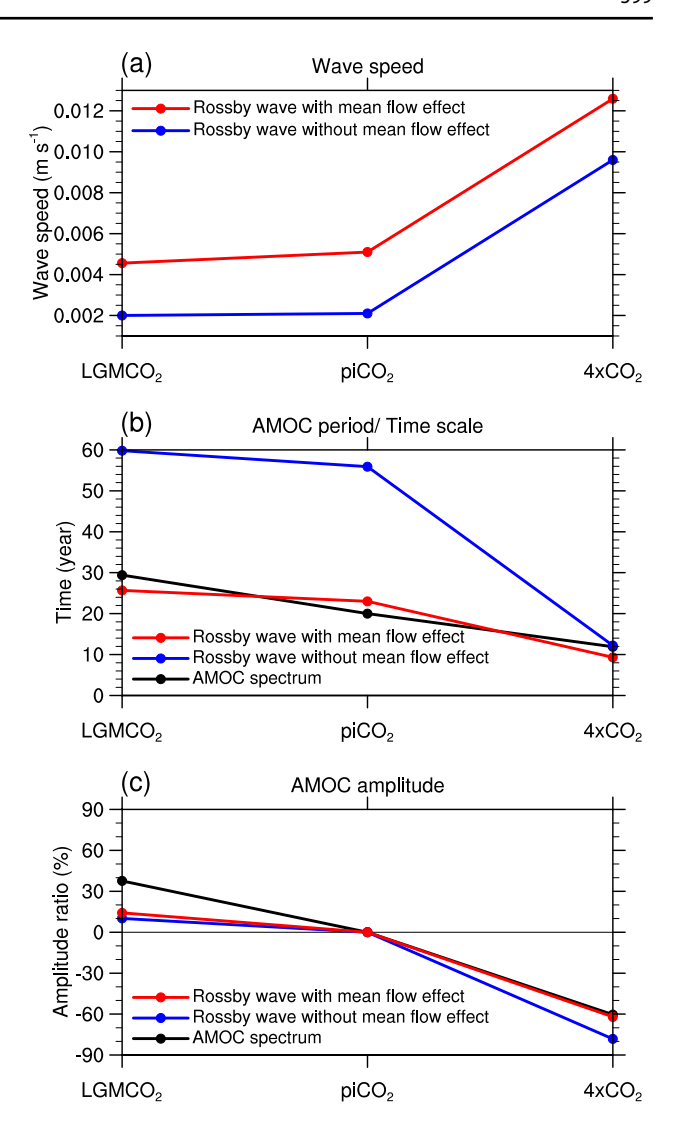


Fig. 5 The changes in ocean baroclinic Rossby wave properties and AMOC variability across the LGMCO₂, piCO₂, and $4 \times \text{CO}_2$ simulations. a Rossby wave speeds without (blue) and with the mean flow effects (red). b the main AMOC periods derived from AMOC spectrum (black), as well as the time scales for the waves to propagate across the Atlantic basin derived from Rossby wave speed without (blue) and with the mean flow effects (red). c AMOC major amplitude ratios (relative to piCO₂) as estimated from AMOC spectrum (black), derived from Rossby wave speed without (blue) and with the mean flow effects (red)

to speculate that other processes might play a role in AMOC variability, especially considering the mode for baroclinic Rossby waves here does not account for convection changes and mean flow effects.

The effect of mean flow is potentially a key factor modulating the westward propagation of temperature or density anomalies in the subpolar North Atlantic. In a continuously stratified ocean, the propagation of Rossby waves could be modulated by effects of mean flow including the mean eastward zonal advection and an additional westward advection



(geostrophic self-advection) (Sévellec and Fedorov 2013, 2015; Ortega et al. 2015), which was initially described in the paradigm of the non-Doppler shift effect (Rossby 1939; Held 1983; Killworth et al. 1997; Liu 1999). Particularly, based on an idealized two-layer model formulated in Sévellec and Fedorov (2013, 2015), in the presence of mean zonal flow, the Rossby wave speed in Eq. (4) can be expressed as

$$c = U - U' - \frac{\beta}{\lambda} \tag{6}$$

with negative signs denoting westward speed direction. U denotes the speed value of mean zonal advection. U'denotes the speed value of geostrophic self-advection.

In our demonstration, we simply consider the change of U averaged between 0 and 1000 m depth for each simulation. We expand the expression of geostrophic self-advection U' denoted by temperature anomalies as in Sévellec and Fedorov (2013) to the form denoted by density anomalies as

$$U' = \frac{gh\widetilde{h}}{2Hf_0} \frac{1}{\rho_0} \frac{\partial \overline{\rho}}{\partial y} \tag{7}$$

where g is gravitational acceleration and ρ is the climatological ocean density. Here, $\tilde{h} = H - h$, indicates the difference between the mean total depth of the ocean (H) and the thickness of the upper ocean (h) in the subpolar North Atlantic. In our estimate, we set H = 4000 m based on the topography of the subpolar North Atlantic (Fig. 1) and set h = 1000 m because the maximum mean AMOC mainly occurs above ~ 1000 m depth (Fig. 1) and ocean stratification has the most prominent changes above ~ 1000 m depth (Fig. 3). We then consider the change of U' in 0-1000 m depth.

Figure 6 shows the mean zonal advection and geostrophic self-advection in the upper 1000 m depth in the North Atlantic. All three simulations exhibit a robust eastward mean flow extending northward to 50°N as contributed by the Gulf Stream and the North Atlantic Current (Fig. 6a–c). The magnitude of the eastward mean flow diminishes with

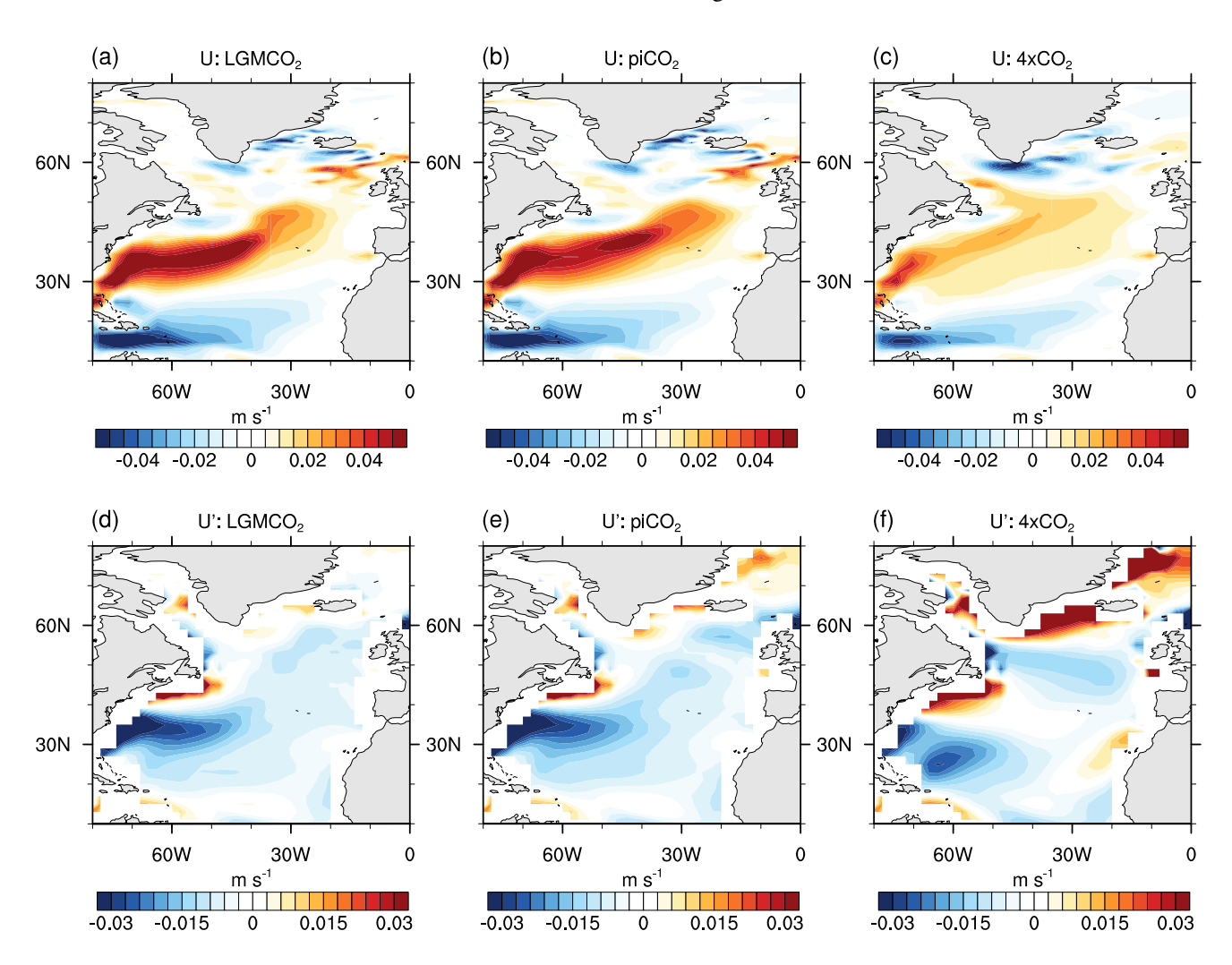


Fig. 6 The mean zonal flow U (top row) and geostrophic self-advection U' (bottom row) in the LGMCO₂ (left column), piCO₂ (middle column), and $4 \times \text{CO}_2$ (right column) simulations, which are averaged over 0–1000 m depth and across the 500-year period



increasing CO₂. On the other hand, the geostrophic self-advection exhibits westward velocities in broad areas over the North Atlantic, with relatively large value along the Gulf Stream and the North Atlantic Current (Fig. 6d, e, f), which acts to cancel part of the local eastward mean flow.

We then average the velocities of mean zonal advection and geostrophic self-advection over the region of 45° N–60° N, 80° W–0°, 0–1000 m depth and recalculate the speed of Rossby wave based on Eq. (6). We find the total mean flow effects increase the Rossby wave speed by a factor of 2.3, 2.4, and 1.3 in the LGMCO₂, piCO₂, and 4×CO₂ simulations (Fig. 5a, red). Correspondingly, the duration for Rossby waves traveling across the Atlantic basin are 25.7, 23.0, and 9.3 years, respectively (Fig. 5b, red). These durations are much closer to the AMOC variability periods estimated from the power spectrum (29.4, 20.0, and 11.9 years) than previous estimates based on the Rossby wave without mean flow effects (59.8, 55.9, and 12.2 years). These results indicate an important role of the mean flow effects in setting the dominant period of AMOC multidecadal variability.

3.2.2 Amplitude

The weakened amplitude of AMOC multidecadal variability in a warming climate might be due to changes in the amplitude of atmospherically-forced oceanic baroclinic Rossby wave. The oceanic baroclinic Rossby wave response forced by surface wind stress can be described by the linearized QGPV equation in the longwave approximation for a two-layer model (after neglecting non-linear perturbation terms) (LaCasce 2000; Cheng et al. 2016) as

$$\partial_t \Psi - \beta R^2 \partial_x \Psi = \frac{R^2}{\rho_0} \nabla \times \tau \tag{8}$$

with R denoting the internal deformation radius and $\nabla \times \tau$ denoting the surface wind-stress curl. The Eq. (8) then can be written as

$$\partial_t \Psi + c \partial_x \Psi = Q \tag{9}$$

where c denotes the Rossby wave speed and Q denotes the atmospheric forcing proportional to the wind-stress curl. Taking the Fourier transform of Eq. (9) leads to.

$$|\widehat{\Psi}|^2 = \frac{|\widehat{Q}|^2}{\omega^2 + c^2 k^2} \tag{10}$$

where the hats denote the Fourier space (frequency domain). ω is circular frequency, and k is zonal wavenumber. This expression indicates that the amplitude $(|\widehat{\Psi}|)$ of the forced Rossby wave is affected by the strength of the atmospheric

forcing Q and the characteristics (ω, c, k) of Rossby wave itself.

As we demonstrated above, when CO_2 concentration rises, the Rossby wave speed c increases, leading to a decrease in Rossby wave time scale T, which induces an increase in circular frequency ω . In our AMOC variability analysis regarding a specific large-scale oceanic Rossby wave in the subpolar North Atlantic, the zonal wavenumber k can be considered the same in the three simulations ($k \approx 1.7 \times 10^{-6}$ m⁻¹ in all cases according to the simple calculation from $k = \omega/c$). Thus, the only unknown term in Eq. (10) is the atmospheric forcing Q.

To evaluate the atmospheric forcing Q, we examine the leading mode of atmospheric variability in the North Atlantic region—the NAO. Here, the NAO index is adopted as the principal component time series of the leading empirical orthogonal function (EOF) of annual mean sea level pressure anomalies over the Atlantic sector (10° N-80° N, 100° W-40° E) (Hurrell 1995; Wen et al. 2016). We find that the amplitudes of the NAO hardly alter among the three cases both from the major spectral peaks (Fig. 2b) and from the EOF analysis (Fig. 7). Therefore, the atmospheric forcing O in Eq. (10) can be seen as largely unchanged under CO₂ increasing, such that the forced Rossby wave amplitude tends to decline as the wave speed and circular frequency increasing and the wavenumber being almost constant. Note that dominant periods of the NAO are 24.6, 37.8, and 25.9 years respectively for the LGMCO₂, piCO₂, and $4 \times CO_2$ simulations (Fig. 2b), which are different from the dominant AMOC periods (29.4, 20.0, 11.9 years) in the three simulations. This lack of agreement between the two sets of dominant periods to some extent excludes the possibility of a near-resonant AMOC response to NAO forcing (Delworth and Zeng 2016) in all cases.

Specifically, we are able to estimate the strength of the atmospheric forcing Q from the amplitude of NAO spectrum peak (Fig. 2b). According to Eq. (10), we then calculate the amplitude change ratio of the forced oceanic Rossby wave in each simulation relative to that in piCO $_2$ (Fig. 5c, blue). The forced Rossby wave amplitude increases by 10.1% in LGMCO $_2$ and decreases by 78.2% in 4 × CO $_2$ relative to that in piCO $_2$. This result is consistent with the reduced amplitude of AMOC spectrum peak with increasing CO $_2$, i.e., +37.6%, 0%, and -60.4% for changes in LGMCO $_2$, piCO $_2$, and $4 \times$ CO $_2$ (Fig. 5c, black).

Furthermore, when the mean flow effects are taken into account, the amplitude change ratio of the forced Rossby wave can be recalculated based on the wave speed in Eq. (6). As a result, the amplitude of the forced Rossby wave increases by 14.2% in LGMCO₂ and decreases by 62.1% in $4\times CO_2$ from that in piCO₂ (Fig. 5c, red), which better resembles the ratio change of the AMOC major amplitude than our previous estimate that based on the Rossby wave without mean flow effects (Fig. 5c, blue). This finding



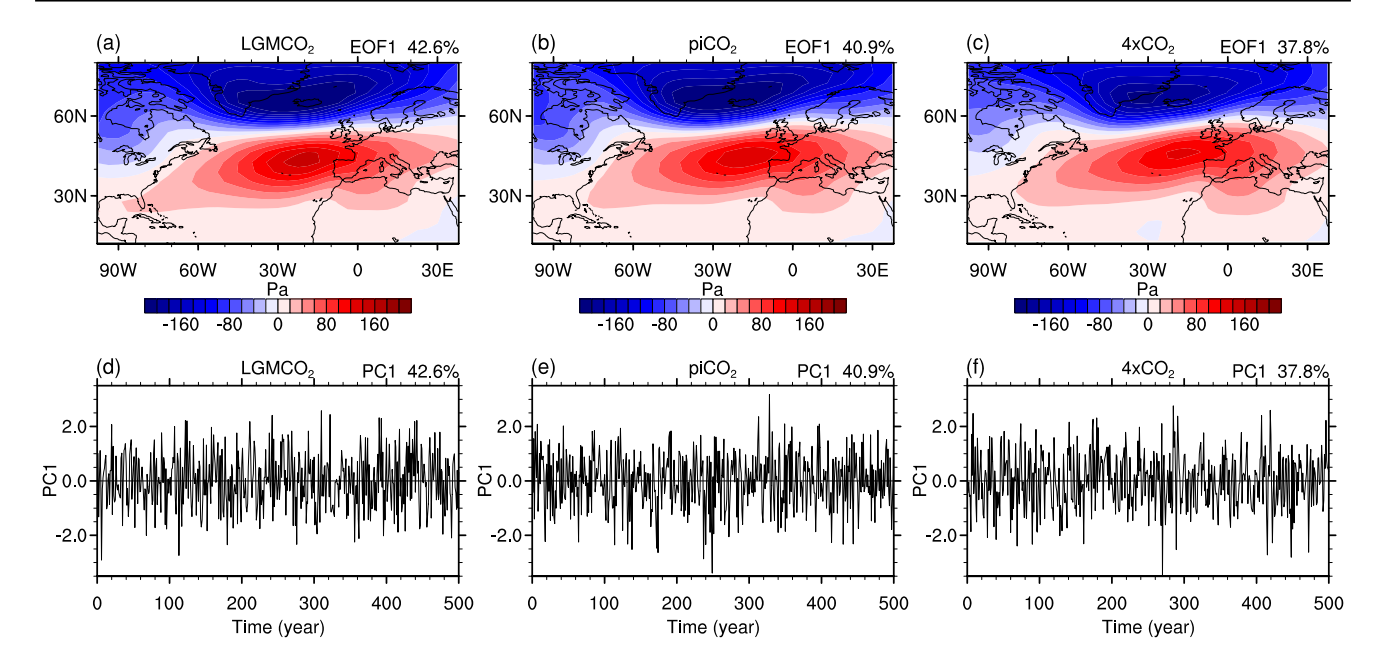


Fig. 7 Spatial patterns and time series of the NAO in the LGMCO₂ (left column), $piCO_2$ (middle column), and $4\times CO_2$ (right column) simulations. The NAO here is calculated from empirical orthogonal function (EOF) of annual mean sea level pressure (SLP) anomalies over the Atlantic sector (10° N– 80° N, 100° W– 40° E). Spatial pat-

terns shown here are regressions of SLP on the normalized leading principal component (PC1) of the leading EOF (EOF1). Time series shown here are the normalized PC1. The explained variance of the leading EOF mode in each simulation is noted on the top of each plot

confirms the importance of mean flow effects in estimating changes in AMOC variability, not only changes in the period but also in the magnitude.

3.3 The phasing of upper ocean temperature change in relation to AMOC oscillations

We further explore the phasing of upper ocean temperature changes associated with AMOC variations to demonstrate the oscillatory behavior of AMOC multidecadal variability in our LGMCO₂, piCO₂, and $4 \times CO_2$ simulations. We first calculate the cross-correlation between the AMOC index at 45° N and upper ocean temperatures (0-1000 m depth) averaged in the subpolar North Atlantic after applying a band-pass filter centered around the AMOC spectral peaks within each simulation (see Fig. 4 caption). We find similar periodic patterns of the correlation between the AMOC and upper ocean temperature within all three simulations (Fig. 8). In the LGMCO₂ simulation (Fig. 8a), the positive correlation between the AMOC and upper ocean temperature has a maximum when the former leads the latter by 11 years, which means a strengthened AMOC produces warm anomalies in the subpolar North Atlantic. On the other hand, the negative correlation between the AMOC and upper ocean temperature has a maximum when the former lags the latter for 4 years, which means that warm anomalies in the subpolar North Atlantic cause weakened AMOC. In the piCO₂ simulation (Fig. 8b),

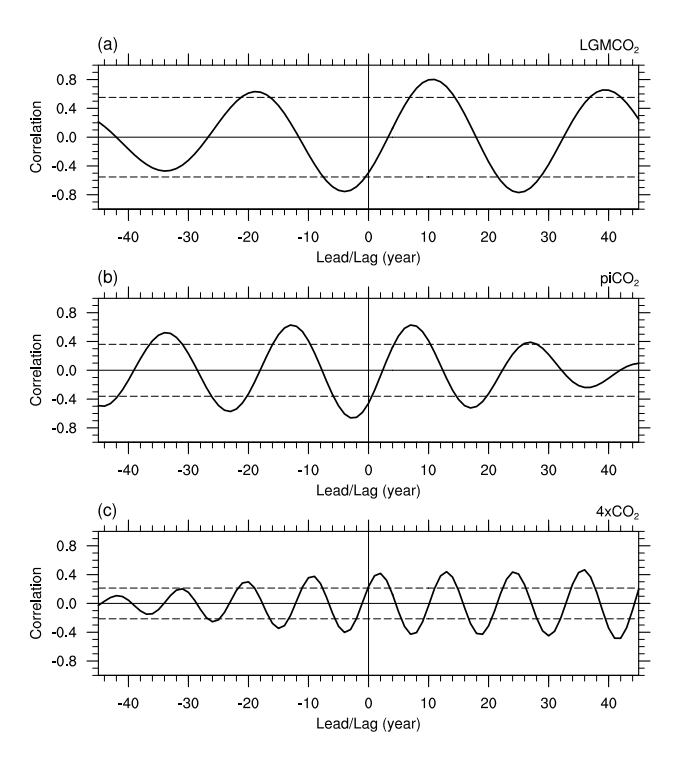


Fig. 8 Cross-correlations between AMOC index at 45° N and upper ocean temperature in the subpolar North Atlantic in the **a** LGMCO₂, **b** piCO₂, and **c** $4 \times \text{CO}_2$ simulations. Positive values in the x-direction denote AMOC leading temperature. Temperatures are averaged over 45° N -60° N, 80° W -0° , 0-1000 m depth. Dash lines denote 95% confidence levels based on the Student's t-test. A band-pass filter centered around the AMOC spectral peak is applied in each simulation (same as used in Fig. 4) before calculating the correlation



there are positive and negative correlation maximums at lags + 7 and -3 (the positive lag denotes AMOC leading temperature). In the $4 \times \text{CO}_2$ simulation (Fig. 8c), positive and negative correlation maximums occur at lags + 2 and -4. Our finding that enhanced AMOC leads to warm anomalies in the subpolar North Atlantic is consistent with previous studies (Zhang 2008; Zhang and Wang 2013; Zhang and Zhang 2015; Yeager and Robson 2017; Sun et al. 2019; Zhang et al. 2019).

To illustrate the temporal evolution of the three-dimensional pattern in upper ocean temperature related to AMOC variations, we regress either the average temperature within 0-1000 m depth or the zonal mean temperature in the North Atlantic onto the AMOC index at 45° N at different lags according to the phasing in Fig. 8. These lags herein define four phases in a period within each simulation. Taking the piCO₂ simulation as an example (Fig. 9). Phase 1 (when temperature lags the AMOC by 2 years) is characterized by a strong east-west temperature gradient within 0-1000 m depth in the North Atlantic between 40° N and 60° N, with negative and positive anomalies appearing in the western and eastern parts of the basin (Fig. 9a). Zonally averaged, the signals of temperature change are weak due to the cancellation between positive and negative anomalies (Fig. 9e). Stepping forward in time about a quarter period, phase 2 features large-scale positive temperature anomalies within 0-1000 m depth in the subpolar North Atlantic (Fig. 9b), which is also evident from the zonal mean view (Fig. 9f).

As we go forward to phase 3 and phase 4, we find that temperature patterns are generally similar to those in phase 1 and phase 2 but with opposite signs (Fig. 9c, d, g, h), which indicates the oscillatory characteristics of Atlantic temperature changes associated with AMOC variations.

We further elaborate on the physical processes and mechanisms linking Atlantic temperature changes to AMOC variations. Starting from phase 4 of the oscillation (Fig. 9d), the large-scale cooling anomalies in the upper ocean occur along with a basin-scale anomalous cyclonic ocean circulation in the subpolar Atlantic. The anomalous circulation acts on the background mean meridional temperature gradient, leading to cold advection from the north on the western side and warm advection from the south on the eastern side. This process, together with the β -effect (df/dy, which is a typical mechanism of the westward propagating baroclinic Rossby wave in the Northern Hemisphere), leads to a westward propagation of cooling anomalies. Again, the propagation of the cooling temperature anomalies involves the interplay between baroclinic Rossby waves and the mean flow effect. Since the cooling is ubiquitous in the subpolar North Atlantic, it does little to alter the zonal density gradient and hardly contributes to the meridional overturning circulation owing to the thermal wind balance. When the cooling anomalies propagate westward and the warm water accumulates on the east side, a dipole of temperature anomalies develops in the subpolar North Atlantic—cooling on the west and warming on the east—which is most pronounced in the next phase,

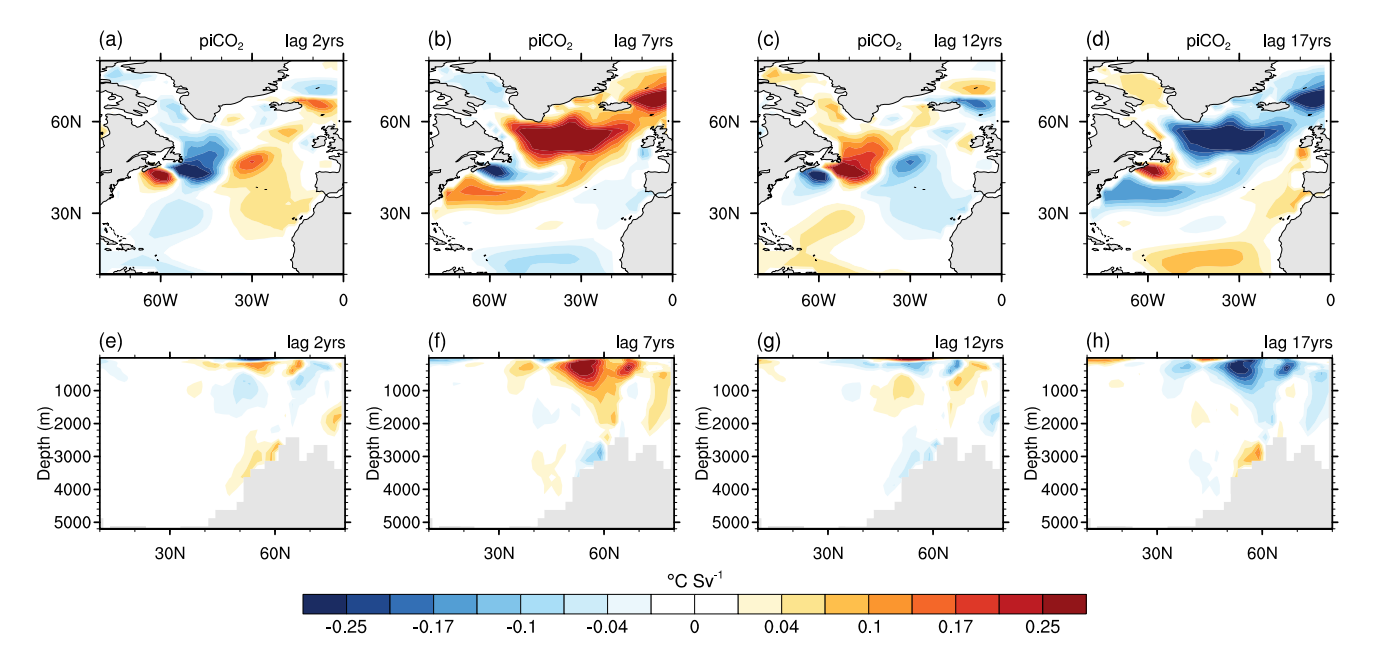


Fig. 9 Phase transformations of upper ocean temperatures in the North Atlantic related to AMOC oscillations in the $piCO_2$ simulation. Regressions of 0–1000 m depth ocean temperatures (top row) and zonal mean ocean temperatures (bottom row) on AMOC index at

 45° N at four phases with different time lags. Time lag for each phase is noted on top of each plot. A band-pass filter around AMOC spectral peak in the piCO₂ simulation is applied (same as used in Fig. 4) before the calculation of regression



namely, phase 1. During phase 1 (Fig. 9a), the dipole-like temperature anomalies create a positive zonal density gradient and engender anomalous northward transports in the upper ocean via the thermal wind relationship, which acts to strengthen the meridional overturning circulation. Via an enhanced northward heat transport, the stronger AMOC subsequently results in general warming over the subpolar North Atlantic, bringing temperature changes into the pattern of phase 2, which is similar to phase 4 but with a reversed sign

(Fig. 9b). The AMOC-related upper ocean temperature then starts the opposite phase of the cycle (Fig. 9b, c).

Similar features of phase changes in upper ocean temperature anomalies related to AMOC variations can also be found in the subpolar North Atlantic in the LGMCO $_2$ (Figs. 10) and 4 × CO $_2$ (Fig. 11) simulations. In short, we find a common feature across all the three simulations that upper ocean temperature anomalies in the subpolar North Atlantic alternate between a one-sign field and a zonal

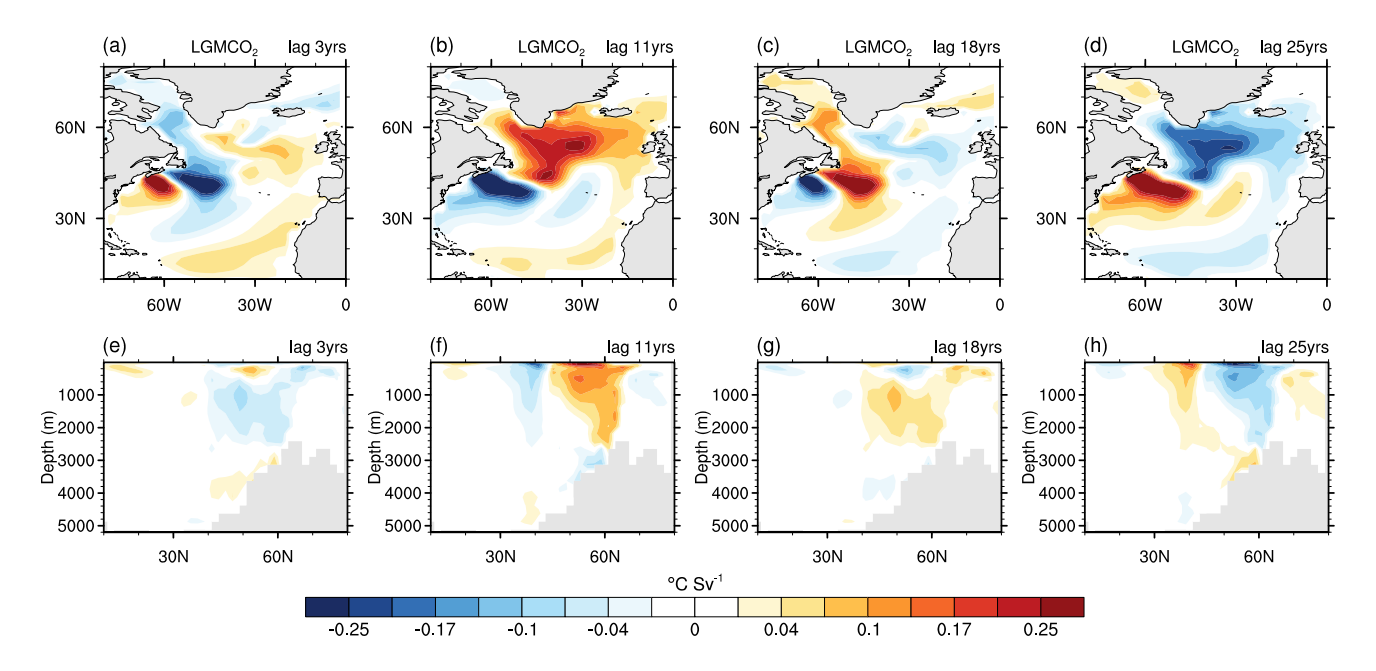


Fig. 10 Same as Fig. 9, but for the $LGMCO_2$ simulation

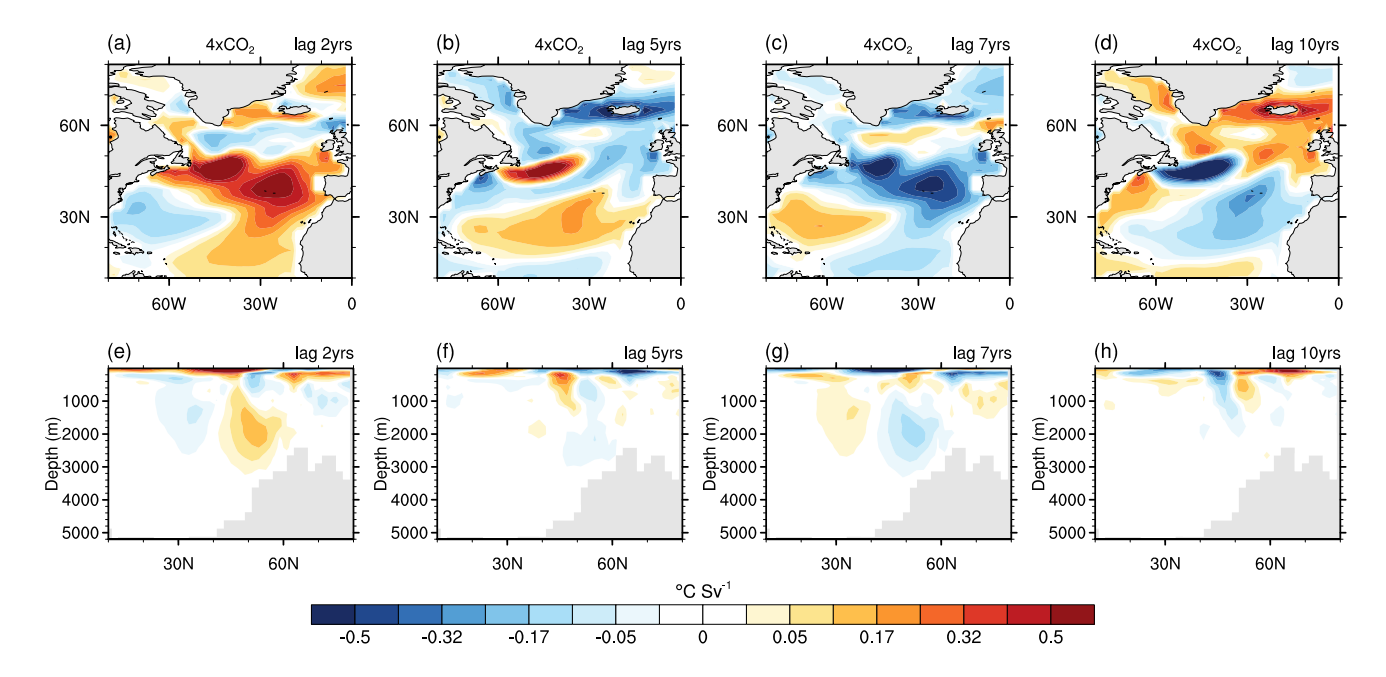


Fig. 11 Same as Fig. 9, but for the $4 \times CO_2$ simulation



dipole in successive time phases, contributing to the periodic oscillation of the AMOC, which is consistent with AMOC-related temperature or density phasing as illustrated in many studies (Colin de Verdiere and Huck 1999; Te Raa and Dijkstra 2002; Tulloch and Marshall 2012; Sévellec and Fedorov 2013, 2015; Ortega et al. 2015; Arzel et al. 2018; Arzel and Huck 2020). It is worth noting that the temperature pattern in the $4 \times CO_2$ simulation is less obvious than those in the LGMCO₂ and piCO₂ simulations, which might be, at least partially, related to the suppressed AMOC variability under $4 \times CO_2$ conditions (Fig. 2a).

3.4 The NAO and AMOC multidecadal variability

To explore the potential interactions between atmospheric forcing and oceanic processes associated with AMOC variability, we examine the relationship between the NAO and

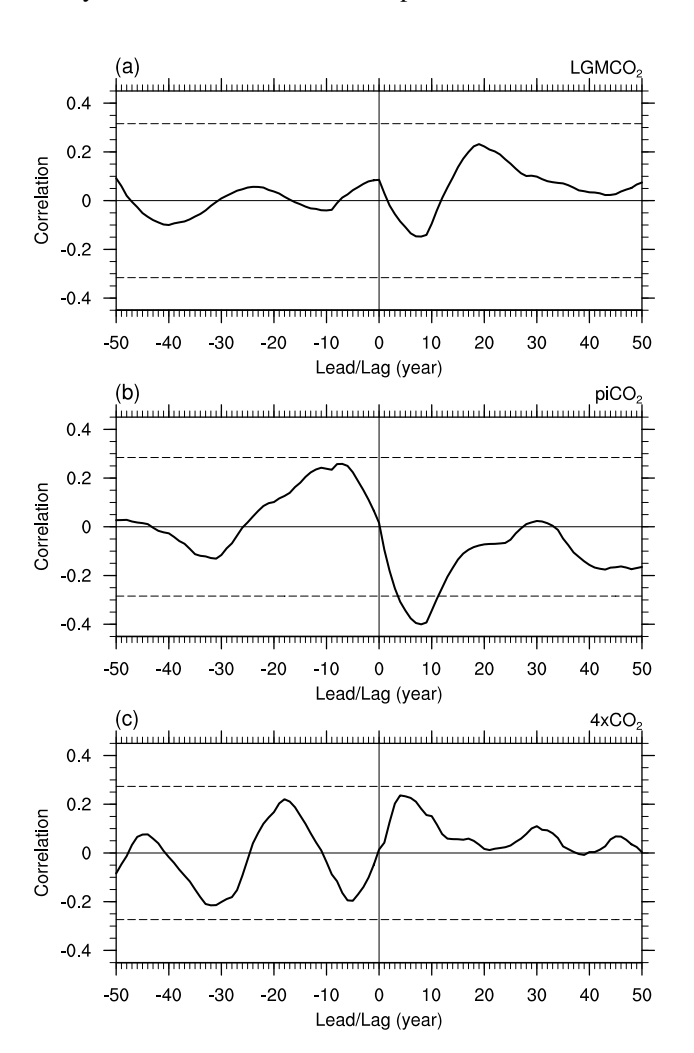


Fig. 12 Cross-correlations between AMOC index and NAO index in the a LGMCO₂, **b** piCO₂, and **c** $4 \times CO_2$ simulations. Positive values in the x-direction denote NAO leading AMOC. Dash lines denote 95% confidence levels based on the Student's t-test. A 9-year running mean is applied to the indices before the calculation of correlation

the AMOC in the LGMCO₂, piCO₂, and $4 \times \text{CO}_2$ simulations (Fig. 12). In the piCO₂ simulation, the lead-lag correlation between the AMOC index and the NAO index shows significant negative correlations only when the NAO leads the AMOC by 3–11 years, with the correlation peaking at a lead of 8 years (Fig. 12b).

To investigate how the NAO affects AMOC fluctuations in the piCO₂ simulation, we regress multiple variables on the NAO index. We find that associated with a positive phase of NAO are negative wind stress curl anomalies centered in the subpolar North Atlantic (Fig. 13a), which drive clockwise anomalous flows in the subpolar gyre (Fig. 13b). The weakened subpolar gyre leads to less warm and salty waters being transported from subtropics to subpolar regions, thus leading to cooling anomalies of sea surface temperature and negative anomalies of sea surface salinity in the subpolar region (Fig. 13c, d). As seen from the contribution of temperature or salinity anomalies to the density anomalies related to NAO variations, the haline effect mostly dominates the change in sea surface density in the subpolar North Atlantic (Fig. 13c, d, e). The freshening anomalies primarily reduce sea surface density to the south of Iceland and inhibit deep convection there (Fig. 13e). This leads to a weakened AMOC at lower latitudes after several years (Fig. 13f) along with the meridional propagation of anomalies in form of advection through interior pathways and coastal Kelvin waves (Zhang 2010). A caveat in this model is that deep convection sites are not very well represented with no strong deep convection in the Labrador Sea as found in observations (Heuzé 2017; Sgubin et al. 2017; Liu et al. 2019). Indeed, the deep convection sites have a large diversity in models (Heuzé 2017; Menary and Wood 2018; Liu et al. 2019). The positive NAO tends to increase sea surface density over the Labrador Sea (Fig. 13e), which should normally enhance deep convection and then the AMOC if the Labrador Sea has active deep convection as found in model studies (Danabasoglu et al. 2012; Gastineau and Frankignoul 2012; Wen et al. 2016; Delworth et al. 2016; Delworth and Zeng 2016; Ortega et al. 2017).

In contrast to the $piCO_2$ simulation, the lead-lag correlations between the NAO and the AMOC are insignificant in the LGMCO₂ and $4 \times CO_2$ simulations (Fig. 12a, c), suggesting that the relationship between the NAO and the AMOC variability may depend on background climate. Moreover, we do not find significant feedbacks of the AMOC on the NAO in all three simulations (Fig. 12), which suggests little active interaction between the AMOC and the NAO in the CESM1-CN. This result may be complementary to previous studies which indicated that the relation between the AMOC and the NAO is model dependent. Particularly, the impacts of AMOC variability on the NAO through the SST footprint (i.e., Atlantic Multidecadal Variability) of the AMOC and the associated anomalies of surface heat flux when the AMOC leads by several years, which have been discussed in



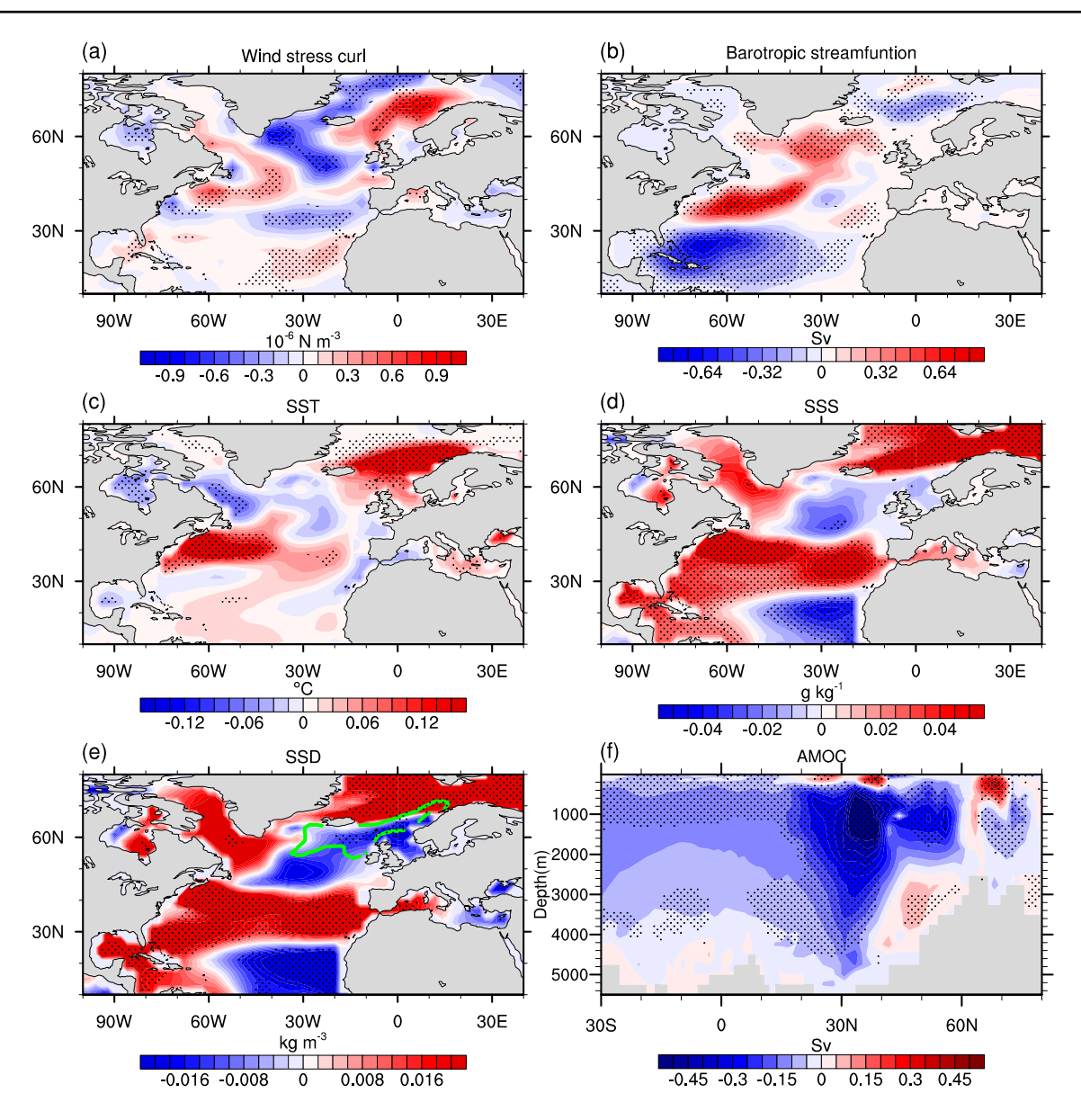


Fig. 13 Regressions when NAO leads AMOC for 8 years on NAO index of **a** wind stress curl, **b** barotropic streamfunction, **c** sea surface temperature, **d** sea surface salinity, **e** sea surface density, and **f** Atlantic meridional overturning streamfunction in the $piCO_2$ simulation. The green contour in **e** denotes the 300-m contour of the 500-year

averaged March mixed layer depth. Stippling denotes where regressions are statistically significant at 95% confidence level based on the Student's t-test. A 9-year running mean is applied to NAO index before the calculation of regression

multiple models (Farneti and Vallis 2011; Sutton et al. 2018; Sun et al. 2019; Zhang et al. 2019; Oelsmann et al. 2020).

4 Conclusion and discussion

Based on coupled climate model simulations, our study investigates the characteristics and physical mechanisms of changes in AMOC variability on multidecadal timescales under different atmospheric CO₂ conditions. We consider three 500-year simulations with atmospheric CO₂

concentrations of 185, 280, and 1120 ppm (LGMCO₂, piCO₂, and $4 \times \text{CO}_2$) and analyze the changes in spectral properties of AMOC variability in the three simulations. We then propose a framework to interpret part of these changes in spectral properties based on the oceanic baroclinic Rossby wave characteristics, as well as the mean flow effects on wave characteristics.

We find that, as CO₂ increases, the period of AMOC variability is shortened and the amplitude of AMOC variability is reduced. With increasing CO₂, the timescale of westward propagating Rossby waves in the subpolar North Atlantic



tends to reduce because the speed of Rossby waves tends to accelerate due to enhanced oceanic stratification. This decreased wave timescale is basically consistent with the shortened period in AMOC variability. On the other hand, the amplitude of atmospherically-forced Rossby waves in the subpolar North Atlantic tends to decrease due to the increase of wave speed and the largely steady strength of NAO forcing under increasing CO₂. This declined wave amplitude is also generally consistent with the weakened magnitude in AMOC variability. Here, we would like to highlight the effects of mean flow that include eastward mean advection and westward geostrophic self-advection. We find that mean flow effects play an important role in modulating the Rossby wave characteristics and in turn the AMOC variability in a continuously stratified ocean mainly through increasing the speed of Rossby waves, which is in line with previous studies (Sévellec and Fedorov 2013, 2015; Ortega et al. 2015). In other words, by considering mean flow effects, we could more accurately estimate the period and amplitude changes in AMOC multidecadal variability under warming climates.

Our analysis has focused on the westward propagation of temperature anomalies associated with AMOC variability rather than salinity anomalies or density anomalies. Some studies have shown that salinity anomalies have similar patterns and propagating characteristics as temperature anomalies, which could to a small extent offset the effect of temperature on AMOC variations (Sévellec and Fedorov 2013, 2015). Other studies have found AMOC-related density anomalies propagating westward in the subpolar North Atlantic in different models (Tulloch and Marshall 2012; Ortega et al. 2015). In fact, several studies have shown that there is quite a bit of diversity among CMIP5 models as to whether temperature or salinity dominant density changes in the subpolar North Atlantic (Menary et al. 2015a, b). Examining the features of salinity anomalies or density anomalies associated with AMOC variability in CESM1-CN will be the focus of future studies.

We use atmospherically-forced Rossby wave to demonstrate the amplitude reduction in AMOC multidecadal variability under different CO₂ forcings. Even if the mean flow effect is included, the amplitude ratio changes estimated from forced waves still do not perfectly fit those calculated from the AMOC spectrum (Fig. 5c). This might be related to our assumption of constant mean zonal flow when we calculate Rossby wave speed with mean flow effects, which indicates that the variation of wave amplitude is only a function of ocean stratification. However, the baroclinic wave amplitude could also be influenced by the vertical shear of the mean flow in turn the baroclinic instability (Colin de Verdière and Huck 1999). The growth rate of baroclinic instability could be evaluated in the simplest case using the Eady growth rate (f/N)dU/dz (Huck et al. 2001) or by doing a complete local linear stability analysis (Arzel et al. 2018).

In our three simulations, the vertical shear of the mean zonal flow (dU/dz) is largely unchanged over the subpolar North Atlantic (not shown), so that other physical processes than the baroclinic instability might also contribute to the AMOC amplitude change since the estimated ratio changes are not perfectly fitting to the spectral results (Fig. 5c).

A number of different mechanisms have been proposed to be responsible for AMOC variability, which, however, heavily depends on the model used and the timescale of focus (Liu 2012; Buckley and Marshall 2016). Our findings of mechanisms in AMOC multidecadal variability are from the perspective of Rossby wave theory based on one model. Another well-known potential mechanism related to density anomalies over deep convection sites mainly driving AMOC multidecadal oscillations has been widely applied in multiple models (Delworth et al. 1993; Griffies and Tziperman 1995; Delworth and Greatbatch 2000; Dai et al. 2005; Dong and Sutton 2005; Danabasoglu 2008; Danabasoglu et al. 2012; Gastineau and Frankignoul 2012; Ortega et al. 2015). A reconciliation between the two mechanisms has been illustrated in IPSL-CM5A (Ortega et al. 2015), in which baroclinic Rossby waves and convection site density anomalies work together to modulate the AMOC variability. Further investigations applying convection site analyses and considering the cooperation between the two mechanisms might be helpful to further improve the estimate of period and amplitude changes in AMOC multidecadal variability under a warming climate.

The NAO in our simulations has significant peaks on multidecadal timescales (24.6, 37.8, and 25.9 years for LGMCO₂, piCO₂, and $4 \times \text{CO}_2$), which is consistent with other studies finding strong NAO decadal variability in observations or models (Li and Wang 2003; Danabasoglu 2008). Since the atmosphere has a very short memory, the decadal variability of the NAO might be related to the interactions between the atmosphere and ocean-cryosphere system (Danabasoglu 2008). The decreasing amount of variance explained by the leading EOF of sea level pressure over the North Atlantic with increasing CO₂ (Fig. 7) may reflect some adjustments of atmosphere internal variability under climate change.

Here we find relatively small impacts of the NAO on AMOC fluctuations in the fully-coupled CESM1-CN model. However, previous studies have indicated, also in a qualitative manner, that NAO variations have large impacts on the AMOC or North Atlantic variability on interannual to multidecadal timescales in multiple models (Timmermann et al. 1998; Delworth and Greatbatch 2000; Eden and Willebrand 2001; Kwon and Frankignoul 2012; Gastineau and Frankignoul 2012; Li et al. 2013; Wen et al. 2016; Delworth et al. 2016). Ocean-only or coupled model experiments forced by NAO-related surface fluxes (Delworth and Greatbatch 2000; Delworth and Zeng



2016; Gastineau et al. 2018; Oelsmann et al. 2020) can be used to determine, in a quantitative manner, the contribution of the changes in atmospheric forcing to ocean variability. Additional diagnostics in a more systematic way by computing the key terms related to atmospheric and oceanic perturbations in the buoyancy variance equation (Gastineau et al. 2018; Arzel and Huck 2020) are also helpful to quantitatively identify the relative role of surface forcing versus internal ocean dynamics.

Acknowledgements XM and GH were supported by CAS COMS2019Q03 and NSFC (41831175, 91937302 and 41721004). NJB was supported by NSF Award OCE-1756658 and a Sloan Ocean Fellowship. We thank the three anonymous reviewers for their thoughtful comments, which helped to improve the manuscript. We are grateful to Peng Hu and Yihua Lin for the valuable discussions on the topic. We thank the development group from the National Center for Atmospheric Research for making their model freely available. Data used in the paper are available from authors upon request.

References

- Armstrong E, Valdes P, House J, Singarayer J (2017) Investigating the impact of CO_2 on low-frequency variability of the AMOC in HadCM3. J Clim 30:7863–7883
- Arzel O, Huck T (2020) Contributions of atmospheric stochastic forcing and intrinsic ocean modes to North Atlantic Ocean interdecadal variability. J Clim 33:2351–2370
- Arzel O, Huck T, Colin de Verdière A (2018) The internal generation of the Atlantic Ocean interdecadal variability. J Clim 31:6411–6432
- Brady EC, Otto-Bliesner BL, Kay JE, Rosenbloom N (2013) Sensitivity to glacial forcing in the CCSM4. J Clim 26:1901–1925
- Buckley MW, Marshall J (2016) Observations, inferences, and mechanisms of the Atlantic Meridional Overturning Circulation: a review. Rev Geophys 54:5–63
- Buckley MW, Ferreira D, Campin J-M et al (2012) On the relationship between decadal buoyancy anomalies and variability of the Atlantic meridional overturning circulation. J Clim 25:8009–8030
- Chelton DB, DeSzoeke RA, Schlax MG et al (1998) Geographical variability of the first baroclinic Rossby radius of deformation. J Phys Oceanogr 28:433–460
- Cheng W, Chiang JC, Zhang D (2013) Atlantic meridional overturning circulation (AMOC) in CMIP5 models: RCP and historical simulations. J Clim 26:7187–7197
- Cheng J, Liu Z, Zhang S et al (2016) Reduced interdecadal variability of Atlantic Meridional Overturning Circulation under global warming. PNAS 113:3175–3178
- Colin de Verdière A, Huck T (1999) Baroclinic instability: an oceanic wavemaker for interdecadal variability. J Phys Oceanogr 29:893–910
- Dai A, Hu A, Meehl G et al (2005) Atlantic thermohaline circulation in a coupled general circulation model: unforced variations versus forced changes. J Clim 18:3270–3293
- Danabasoglu G (2008) On multidecadal variability of the Atlantic meridional overturning circulation in the Community Climate System Model version 3. J Clim 21:5524–5544
- Danabasoglu G, Yeager SG, Kwon Y-O et al (2012) Variability of the Atlantic meridional overturning circulation in CCSM4. J Clim 25:5153–5172

- Delworth TL, Greatbatch RJ (2000) Multidecadal thermohaline circulation variability driven by atmospheric surface flux forcing. J Clim 13:1481–1495
- Delworth TL, Zeng F (2008) Simulated impact of altered Southern Hemisphere winds on the Atlantic meridional overturning circulation. Geophys Res Lett 35:L20708
- Delworth TL, Zeng F (2012) Multicentennial variability of the Atlantic meridional overturning circulation and its climatic influence in a 4000 year simulation of the GFDL CM2. 1 climate model. Geophys Res Lett 39:L13702
- Delworth TL, Zeng F (2016) The impact of the North Atlantic Oscillation on climate through its influence on the Atlantic meridional overturning circulation. J Clim 29:941–962
- Delworth T, Manabe S, Stouffer RJ (1993) Interdecadal variations of the thermohaline circulation in a coupled ocean-atmosphere model. J Clim 6:1993–2011
- Delworth TL, Manabe S, Stouffer RJ (1997) Multidecadal climate variability in the Greenland Sea and surrounding regions: a coupled model simulation. Geophys Res Lett 24:257–260
- Delworth TL, Zeng F, Vecchi GA et al (2016) The North Atlantic Oscillation as a driver of rapid climate change in the Northern Hemisphere. Nat Geosci 9:509–512
- Dijkstra HA, Te Raa L, Schmeits M, Gerrits J (2006) On the physics of the Atlantic multidecadal oscillation. Ocean Dyn 56:36–50
- Dong B, Sutton RT (2005) Mechanism of interdecadal thermohaline circulation variability in a coupled ocean–atmosphere GCM. J Clim 18:1117–1135
- Drijfhout S, Hazeleger W, Selten F, Haarsma R (2008) Future changes in internal variability of the Atlantic Meridional Overturning Circulation. Clim Dyn 30:407–419
- Eden C, Willebrand J (2001) Mechanism of interannual to decadal variability of the North Atlantic circulation. J Clim 14:2266–2280
- Enfield DB, Mestas-Nuñez AM, Trimble PJ (2001) The Atlantic multidecadal oscillation and its relation to rainfall and river flows in the continental US. Geophys Res Lett 28:2077–2080
- Escudier R, Mignot J, Swingedouw D (2013) A 20-year coupled oceansea ice-atmosphere variability mode in the North Atlantic in an AOGCM. Clim Dyn 40:619–636
- Farneti R, Vallis GK (2011) Mechanisms of interdecadal climate variability and the role of ocean–atmosphere coupling. Clim Dyn 36:289–308
- Frankcombe L, Dijkstra H (2009) Coherent multidecadal variability in North Atlantic sea level. Geophys Res Lett 36:15: L15604
- Frankcombe L, Dijkstra H (2011) The role of Atlantic-Arctic exchange in North Atlantic multidecadal climate variability. Geophys Res Lett 38:L16603
- Frankcombe L, Dijkstra H, Von der Heydt A (2008) Sub-surface signatures of the Atlantic Multidecadal Oscillation. Geophys Res Lett 35:L19602
- Frankcombe LM, Von Der Heydt A, Dijkstra HA (2010) North Atlantic multidecadal climate variability: an investigation of dominant time scales and processes. J Clim 23:3626–3638
- Frankignoul C, Gastineau G, Kwon Y-O (2013) The influence of the AMOC variability on the atmosphere in CCSM3. J Clim 26:9774–9790
- Gastineau G, Frankignoul C (2012) Cold-season atmospheric response to the natural variability of the Atlantic meridional overturning circulation. Clim Dyn 39:37–57
- Gastineau G, Mignot J, Arzel O, Huck T (2018) North Atlantic Ocean internal decadal variability: role of the mean state and oceanatmosphere coupling. J Geophys Res Oceans 123:5949–5970
- Gill AE (1982) Atmosphere-ocean dynamics. Academic, New York
- Gregory J, Dixon K, Stouffer R et al (2005) A model intercomparison of changes in the Atlantic thermohaline circulation in response



- to increasing atmospheric ${\rm CO_2}$ concentration. Geophys Res Lett 32:L12703
- Griffies SM, Bryan K (1997) Predictability of North Atlantic multidecadal climate variability. Science 275:181–184
- Griffies SM, Tziperman E (1995) A linear thermohaline oscillator driven by stochastic atmospheric forcing. J Clim 8:2440–2453
- Hawkins E, Sutton R (2007) Variability of the Atlantic thermohaline circulation described by three-dimensional empirical orthogonal functions. Clim Dyn 29:745–762
- Held IM (1983) Stationary and quasi-stationary eddies in the extratropical troposphere: theory. Large Scale Dyn Process Atmos 127:168
- Heuzé C (2017) North Atlantic deep water formation and AMOC in CMIP5 models. Ocean Sci 13:609–622
- Holland MM, Bailey DA, Briegleb BP et al (2012) Improved sea ice shortwave radiation physics in CCSM4: the impact of melt ponds and aerosols on Arctic sea ice. J Clim 25:1413–1430
- Hu A, Otto-Bliesner BL, Meehl GA et al (2008) Response of thermohaline circulation to freshwater forcing under present-day and LGM conditions. J Clim 21:2239–2258
- Huck T, Vallis GK (2001) Linear stability analysis of the threedimensional thermally-driven ocean circulation: application to interdecadal oscillations. Tellus A 53:526–545
- Huck T, Vallis GK, Colin de Verdière A (2001) On the robustness of the interdecadal modes of the thermohaline circulation. J Clim 14:940–963
- Hurrell JW (1995) Decadal trends in the North Atlantic Oscillation: regional temperatures and precipitation. Science 269:676–679
- Johnson HL, Marshall DP (2002) A theory for the surface Atlantic response to thermohaline variability. J Phys Oceanogr 32:1121–1132
- Jungclaus JH, Haak H, Latif M, Mikolajewicz U (2005) Arctic-North Atlantic interactions and multidecadal variability of the meridional overturning circulation. J Clim 18:4013–4031
- Kawase M (1987) Establishment of deep ocean circulation driven by deep-water production. J Phys Oceanogr 17:2294–2317
- Killworth PD, Chelton DB, de Szoeke RA (1997) The speed of observed and theoretical long extratropical planetary waves. J Phys Oceanogr 27:1946–1966
- Knight JR, Allan RJ, Folland CK et al (2005) A signature of persistent natural thermohaline circulation cycles in observed climate. Geophys Res Lett 32:L20708
- Knight JR, Folland CK, Scaife AA (2006) Climate impacts of the Atlantic multidecadal oscillation. Geophys Res Lett 33:L17706
- Kwon Y-O, Frankignoul C (2012) Stochastically-driven multidecadal variability of the Atlantic meridional overturning circulation in CCSM3. Clim Dyn 38:859–876
- LaCasce J (2000) Baroclinic Rossby waves in a square basin. J Phys Oceanogr 30:3161–3178
- Latif M, Keenlyside NS (2011) A perspective on decadal climate variability and predictability. Deep Sea Res Part II 58:1880–1894
- Lawrence DM, Oleson KW, Flanner MG et al (2012) The CCSM4 land simulation, 1850–2005: assessment of surface climate and new capabilities. J Clim 25:2240–2260
- Li J, Wang JX (2003) A new North Atlantic Oscillation index and its variability. Adv Atmos Sci 20:661–676
- Li J, Sun C, Jin F (2013) NAO implicated as a predictor of Northern Hemisphere mean temperature multidecadal variability. Geophys Res Lett 40:5497–5502
- Liu Z (1999) Planetary wave modes in the thermocline: non-Doppler-shift mode, advective mode and Green mode. Q J R Meteorol Soc 125:1315–1339
- Liu Z (2012) Dynamics of interdecadal climate variability: a historical perspective. J Clim 25:1963–1995

- Liu W, Liu Z (2013) A diagnostic indicator of the stability of the Atlantic meridional overturning circulation in CCSM3. J Clim 26:1926–1938
- Liu Z, Otto-Bliesner B, He F et al (2009) Transient simulation of last deglaciation with a new mechanism for Bølling-Allerød warming. Science 325:310–314
- Liu W, Xie SP, Liu Z et al (2017) Overlooked possibility of a collapsed Atlantic Meridional Overturning Circulation in warming climate. Sci Adv 3:e1601666
- Liu W, Fedorov AV, Sévellec F (2019) The mechanisms of the Atlantic meridional overturning circulation slowdown induced by Arctic sea ice decline. J Clim 32:977–996
- Liu W, Fedorov AV, Xie SP et al (2020) Climate impacts of a weakened Atlantic Meridional Overturning Circulation in a warming climate. Sci Adv 6:eaaz4876
- Ma X, Liu W, Allen RJ et al (2020) Dependence of regional ocean heat uptake on anthropogenic warming scenarios. Sci Adv 6:eabc0303
- MacMartin DG, Zanna L, Tziperman E (2016) Suppression of Atlantic meridional overturning circulation variability at increased CO₂. J Clim 29:4155–4164
- McManus JF, Francois R, Gherardi J-M et al (2004) Collapse and rapid resumption of Atlantic meridional circulation linked to deglacial climate changes. Nature 428:834–837
- Menary MB, Wood RA (2018) An anatomy of the projected North Atlantic warming hole in CMIP5 models. Clim Dyn 50:3063–3080
- Menary MB, Park W, Lohmann K et al (2012) A multimodel comparison of centennial Atlantic meridional overturning circulation variability. Clim Dyn 38:2377–2388
- Menary MB, Hodson DL, Robson JI et al (2015a) Exploring the impact of CMIP5 model biases on the simulation of North Atlantic decadal variability. Geophys Res Lett 42:5926–5934
- Menary MB, Hodson DLR, Robson JI et al (2015) A Mechanism of Internal Decadal Atlantic Ocean Variability in a high-resolution coupled climate model. J Clim 28:7764–7785
- Msadek R, Frankignoul C (2009) Atlantic multidecadal oceanic variability and its influence on the atmosphere in a climate model. Clim Dyn 33:45–62
- Msadek R, Dixon K, Delworth T, Hurlin W (2010) Assessing the predictability of the Atlantic meridional overturning circulation and associated fingerprints. Geophys Res Lett 37:L19608
- Muir LC, Fedorov AV (2017) Evidence of the AMOC interdecadal mode related to westward propagation of temperature anomalies in CMIP5 models. Clim Dyn 48:1517–1535
- Neale RB, Chen C-C, Gettelman A et al (2010) Description of the NCAR community atmosphere model (CAM 5.0). NCAR Tech Note NCAR/TN-486 + STR 1:1–12
- Oelsmann J, Borchert L, Hand R et al (2020) Linking ocean forcing and atmospheric interactions to Atlantic Multidecadal Variability in MPI-ESM1.2. Geophys Res Lett 47:e2020GL087259
- Ortega P, Montoya M, González-Rouco F et al (2012) Variability of the Atlantic meridional overturning circulation in the last millennium and two IPCC scenarios. Clim Dyn 38:1925–1947
- Ortega P, Mignot J, Swingedouw D et al (2015) Reconciling two alternative mechanisms behind bi-decadal variability in the North Atlantic. Prog Oceanogr 137:237–249
- Ortega P, Robson J, Sutton RT, Andrews MB (2017) Mechanisms of decadal variability in the Labrador Sea and the wider North Atlantic in a high-resolution climate model. Clim Dyn 49:2625–2647
- Park W, Latif M (2008) Multidecadal and multicentennial variability of the meridional overturning circulation. Geophys Res Lett 35:L22703
- Rossby C-G (1939) Relation between variations in the intensity of the zonal circulation of the atmosphere and the displacements of the semi-permanent centers of action. J Mar Res 2:38–55



- Ruprich-Robert Y, Cassou C (2015) Combined influences of seasonal East Atlantic Pattern and North Atlantic Oscillation to excite Atlantic multidecadal variability in a climate model. Clim Dyn 44:229–253
- Sévellec F, Fedorov AV (2013) The leading, interdecadal eigenmode of the Atlantic meridional overturning circulation in a realistic ocean model. J Clim 26:2160–2183
- Sévellec F, Fedorov AV (2015) Optimal excitation of AMOC decadal variability: links to the subpolar ocean. Prog Oceanogr 132:287–304
- Sgubin G, Swingedouw D, Drijfhout S et al (2017) Abrupt cooling over the North Atlantic in modern climate models. Nat Commun 8:14375
- Shields CA, Bailey DA, Danabasoglu G et al (2012) The low-resolution CCSM4. J Clim 25:3993–4014
- Smith R, Jones P, Briegleb B et al (2010) The parallel ocean program (POP) reference manual: ocean component of the community climate system model (CCSM) and community earth system model (CESM). LAUR-01853 141:1–140
- Srokosz M, Bryden H (2015) Observing the Atlantic Meridional Overturning Circulation yields a decade of inevitable surprises. Science 348:1255575
- Sun C, Li J, Kucharski F et al (2019) Contrasting spatial structures of Atlantic Multidecadal Oscillation between observations and slab ocean model simulations. Clim Dyn 52:1395–1411
- Sutton RT, Hodson DL (2005) Atlantic Ocean forcing of North American and European summer climate. Science 309:115–118
- Sutton R, McCarthy GD, Robson J et al (2018) Atlantic multidecadal variability and the UK ACSIS program. Bull Am Meteor Soc 99:415–425
- Te Raa LA, Dijkstra HA (2002) Instability of the thermohaline ocean circulation on interdecadal timescales. J Phys Oceanogr 32:138–160
- Timmermann A, Latif M, Voss R, Grötzner A (1998) Northern Hemispheric interdecadal variability: a coupled air–sea mode. J Clim 11:1906–1931
- Tulloch R, Marshall J (2012) Exploring mechanisms of variability and predictability of Atlantic meridional overturning circulation in two coupled climate models. J Clim 25:4067–4080
- Vellinga M, Wu P (2004) Low-latitude freshwater influence on centennial variability of the Atlantic thermohaline circulation. J Clim 17:4498–4511
- Weaver AJ, Sarachik E, Marotzke J (1991) Internal low frequency variability of the ocean's thermohaline circulation. Nature 353:836-838

- Wen N, Frankignoul C, Gastineau G (2016) Active AMOC–NAO coupling in the IPSL-CM5A-MR climate model. Clim Dyn 47:2105–2119
- Yeager S, Robson J (2017) Recent progress in understanding and predicting Atlantic decadal climate variability. Curr Clim Change Rep 3:112–127
- Yin F, Sarachik E (1995) Interdecadal thermohaline oscillations in a sector ocean general circulation model: advective and convective processes. J Phys Oceanogr 25:2465–2484
- Zhang R (2008) Coherent surface-subsurface fingerprint of the Atlantic meridional overturning circulation. Geophys Res Lett 35:L20705
- Zhang R (2010) Latitudinal dependence of Atlantic meridional overturning circulation (AMOC) variations. Geophys Res Lett 37:L16703
- Zhang R, Delworth TL (2006) Impact of Atlantic multidecadal oscillations on India/Sahel rainfall and Atlantic hurricanes. Geophys Res Lett 33:L17712
- Zhang L, Wang C (2013) Multidecadal North Atlantic sea surface temperature and Atlantic meridional overturning circulation variability in CMIP5 historical simulations. J Geophys Res Oceans 118:5772–5791
- Zhang J, Zhang R (2015) On the evolution of Atlantic Meridional Overturning Circulation Fingerprint and implications for decadal predictability in the North Atlantic. Geophys Res Lett 42:5419–5426
- Zhang R, Sutton R, Danabasoglu G et al (2019) A review of the role of the Atlantic meridional overturning circulation in Atlantic multidecadal variability and associated climate impacts. Rev Geophys 57:316–375
- Zhu X, Jungclaus J (2008) Interdecadal variability of the meridional overturning circulation as an ocean internal mode. Clim Dyn 31:731–741
- Zhu J, Liu Z, Zhang J, Liu W (2015) AMOC response to global warming: dependence on the background climate and response time-scale. Clim Dyn 44:3449–3468

Publisher's note Springer Nature remains neutral with regard to jurisdictional claims in published maps and institutional affiliations.

